Formation and dissolution of bacterial colonies

Christoph A. Weber,[1] Yen Ting Lin,[1] Nicolas Biais,[2] and Vasily Zaburdaev[1]
[1]*Max Planck Institute for the Physics of Complex Systems, Nöthnitzer Str. 38, Dresden 01187, Germany*
[2]*Department of Biology, Brooklyn College, City University of New York, Brooklyn, New York 11210, USA*
(Received 17 October 2014; revised manuscript received 28 May 2015; published 3 September 2015)

Many organisms form colonies for a transient period of time to withstand environmental pressure. Bacterial biofilms are a prototypical example of such behavior. Despite significant interest across disciplines, physical mechanisms governing the formation and dissolution of bacterial colonies are still poorly understood. Starting from a kinetic description of motile and interacting cells we derive a hydrodynamic equation for their density on a surface, where most of the kinetic coefficients are estimated from experimental data for *N. gonorrhoeae* bacteria. We use it to describe the formation of multiple colonies with sizes consistent with experimental observations. Finally, we show how the changes in the cell-to-cell interactions lead to the dissolution of the bacterial colonies. The successful application of kinetic theory to a complex far from equilibrium system such as formation and dissolution of living bacterial colonies potentially paves the way for the physical quantification of the initial stages of biofilm formation.

DOI: 10.1103/PhysRevE.92.032704 PACS number(s): 87.23.Cc, 05.20.Dd, 87.18.Ed, 87.18.Hf

I. INTRODUCTION

Colony formation is a pervasive phenomenon in living systems and is crucial for the survival of many species [1–6]. One of the well-known examples where colony formation is essential are biofilms. A bacterial colony can grow from a single cell via multiple cell divisions [1,5]. However, there is another mechanism, which relies on successive encounters of individual, motile bacteria, as also occurring in the initial stages of biofilm formation. This scenario of a kinetic formation of colonies dominates over proliferation if individuals are highly motile and their encounters drive the assembly of cells on a time scale much shorter than the characteristic cell division time. *N. gonorrhoeae* or *N. meningitidis* on biotic or abiotic substrates such as glass [7], plastic [Fig. 1(a)], or epithelial tissue [3] are prototypical examples for such a scenario. Motility of these and many other bacteria originates from long and thin filaments, called pili, which grow out of the cell, attach to a substrate, retract, and thereby actively pull the cell forward [8–11]. Pili are also used to mediate attractive displacements between cells [7,11–13] with a characteristic interaction scale given by the mean pili length. Colonies begin to form within thirty minutes, which is significantly smaller than the characteristic cell division time scale (*N. gonorrhoeae*: approximately 3 h [14]). Bacterial colonies are in general reversible structures. Under certain conditions, for example, the lack of nutrients or oxygen, they can dissolve and recolonize their surroundings [15–17]. Specifically, *N. meningitidis* and *N. gonorrhoeae* bacterial colonies have been shown to dissolve by effectively lowering the strength of the pili-mediated interaction [16,17].

However, so far, the physical mechanisms governing the formation and dissolution of bacterial colonies are poorly understood. Since motility and interactions are driven by active retractions of pili, fundamental concepts from equilibrium statistical mechanics are in general not applicable. The inherent nonequilibrium nature of this system suggests consideration of a kinetic approach reminiscent of the Boltzmann equation, which has been successfully employed to describe the order-disorder transitions in several active systems far from equilibrium [18–28].

Here we propose a kinetic description as a general framework of how living colonies form and dissolve, which keeps track of the length scales and the specific properties of the interactions between individuals. By a coarse-graining procedure we derive the corresponding hydrodynamic equation and find an ordering instability for a choice of parameters relevant to *N. gonorrhoeae*. It belongs to a class of instabilities, where the diffusion constant is negative and originates from attractive pili-mediated interactions. As most of the parameters can be estimated based on available data for *N. gonorrhoeae*, we analytically compute the corresponding phase diagram and find a characteristic colony size that is consistent with experimental observations.

Our theory can also be used to compare the effects of different cell-cell interactions and investigate their interplay. We show that pili interactions are more effective regarding clustering than cell adhesion. Moreover, when both interactions keep the cells together in the colony, a more efficient and robust way to dissolve the colony is to lower the strength of pili-mediated interactions. This suggests that pili play an essential role not only in cell motility and assembly of colonies,

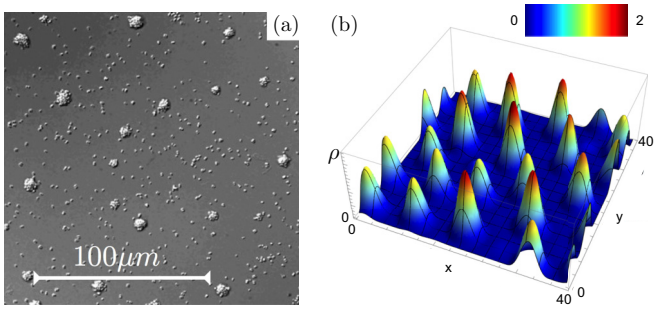

FIG. 1. (Color online) (a) *N. gonorrhoeae* colonies three hours after sedimentation on a plastic substrate. (b) Typical snapshot of the cell density $\rho(x,y)$ as a function of the spatial coordinates x and y, which is obtained from a numerical solution to Eq. (2a). The snapshot corresponds to the regime where colonies grow only very slowly (see Sec. IVB). For a video, please refer to the Supplemental Material [29].

but also in the dissolution of matured colonies. Our results demonstrate that kinetic theory can be applied to quantify the process of colony formation in living systems and is able to provide insights about the underlying physical mechanisms.

II. KINETIC MODEL FOR BACTERIAL COLONY FORMATION

Our kinetic description is formulated in terms of the particle density $f(\mathbf{r},t)$. We restrict ourselves to two-dimensional colonies forming on a planar substrate [30], which do not give rise to swarms or swirls (see, e.g., Ref. [22]). Therefore, the spatial coordinates $\mathbf{r} \in \mathbb{R}^2$ suffice as dynamical variables. In the absence of interactions cells are assumed to move across the substrate by pili-mediated displacements as in the case of *N. gonorrhoeae* or *N. meningitidis*, leading to a diffusive behavior at large length and time scales [31]. Interactions enter the kinetic description via collision rules. A collision rule $\mathcal{R}$ maps the precollision coordinates to the postcollision positions by means of the $\delta(\cdot)$ functions. The corresponding kinetic equation is

$$\partial_t f(\mathbf{r},t) = \mathcal{C}_{\rm mot}(\mathbf{r},t) + \mathcal{C}_{\rm int}(\mathbf{r},t), \tag{1a}$$

where $\mathcal{C}_{\rm mot}$ describes the cell motility across the substrate

$$\mathcal{C}_{\rm mot}(\mathbf{r},t) = \int d\mathbf{r}' [\mathcal{K}_{\mathbf{r}'\to\mathbf{r}} f(\mathbf{r}',t) - \mathcal{K}_{\mathbf{r}\to\mathbf{r}'} f(\mathbf{r},t)] \tag{1b}$$

and $\mathcal{C}_{\rm int}$ accounts for the cell-cell interactions

$$\begin{aligned}\mathcal{C}_{\rm int}(\mathbf{r},t) = \frac{1}{2}\int d\mathbf{r}_1 \int d\mathbf{r}_2\, \mathcal{W}_\square(|\mathbf{r}_{12}|) f(\mathbf{r}_1,t) f(\mathbf{r}_2,t) \\ \times \{\delta[\mathcal{R}_1(\mathbf{r}_1,\mathbf{r}_2) - \mathbf{r}] + \delta[\mathcal{R}_2(\mathbf{r}_1,\mathbf{r}_2) - \mathbf{r}] \\ - 2\delta(\mathbf{r}_2 - \mathbf{r})\}.\end{aligned} \tag{1c}$$

$\mathcal{K}_{\mathbf{r}\to\mathbf{r}'}$ denotes the transition kernel to move from $\mathbf{r}$ to $\mathbf{r}'$ by a retraction event of an individual pilus. We assume that retraction events are independent and that the corresponding rate is isotropic, with a characteristic length scale given by the pili length $\ell_{\rm pi}$. There is experimental evidence that the pili lengths are distributed exponentially [31]. Therefore, we consider the transition kernel

$$\mathcal{K}_{\mathbf{r}\to\mathbf{r}+\mathbf{b}} = \mathcal{K}_0/\left(2\pi\ell_{\rm pi}^2\right) \exp\left(-|\mathbf{b}|/\ell_{\rm pi}\right), \tag{1d}$$

with $\mathcal{K}_0$ denoting the attachment rate of pili to the substrate and $\mathbf{b} = \mathbf{r}' - \mathbf{r}$ is the displacement resulting from an individual pilus retraction.

$\mathcal{W}_\square(|\mathbf{r}_{12}|)$ characterizes the isotropic kernel for collisions between cells with $|\mathbf{r}_{12}| = |\mathbf{r}_1 - \mathbf{r}_2|$ denoting the relative cell-cell distance. For pili-mediated attractive displacements, we consider the following collision rule:

$$(\mathbf{r}_1,\mathbf{r}_2) \to (\mathcal{R}_1,\mathcal{R}_2) = (\mathbf{r}_1 - a\mathbf{r}_{12}, \mathbf{r}_2 + a\mathbf{r}_{12}), \tag{1e}$$

where $a \in [0,1/2]$ is a measure for the strength of the attractive interaction. For $a = 1/2$, cells are maximally attracted, and displaced to the center-of-mass coordinate $\mathbf{R}_{12} = (\mathbf{r}_1 + \mathbf{r}_2)/2$ between the collision partners, while for $a = 0$, cells diffuse freely without interacting. Due to the exponential distribution of the pili lengths, the interaction rate is

$$\mathcal{W}_\square \equiv \mathcal{W}_{\rm pi}(|\mathbf{r}_{12}|) = \gamma\mathcal{W}_0/\left(2\pi\ell_{\rm pi}^2\right) \exp\left(-|\mathbf{r}_{12}|/\ell_{\rm pi}\right), \tag{1f}$$

where $\ell_{\rm pi}$ sets the characteristic length scale for the attractive interaction and $\mathcal{W}_0$ denotes the interaction rate. Since pili-mediated cell-cell interactions are intrinsically stochastic [8,9], we introduce a nondimensional number, γ, accounting for the number of successful binding and retraction events to the total number of pili-cell encounter events.

III. DERIVATION OF HYDRODYNAMIC EQUATION

The isotropy of the interaction rates allows us to integrate Eq. (1) over the center-of-mass coordinates $\mathbf{R}_{12}$ leading to nonlocal terms [see Appendix A]. These terms are related to the length scales of the interactions and resemble a phenomenological description for the assembly of active bundles [32–34]. Since cell colonies typically exhibit sizes noticeably beyond the interaction length scale, the nonlocal integrands can be removed by expanding the particle density f with respect to the spatial coordinates [18,22]. Truncation of this expansion amounts to coarse graining beyond the interaction length scale. To obtain a well-defined set of hydrodynamic equations for the dynamics of bacterial colonies with pili-mediated interactions we truncate at the fourth order [see Appendix B for details]:

$$\begin{aligned}\partial_t\rho(\mathbf{r},t) = \alpha(\rho)\nabla^2\rho(\mathbf{r},t) - \beta_1|\nabla\rho(\mathbf{r},t)|^2 + \kappa(\rho)\nabla^4\rho(\mathbf{r},t) \\ + \beta_2[\nabla^2\rho(\mathbf{r},t)]^2 - \beta_3[\nabla\rho(\mathbf{r},t)]\cdot\nabla^3\rho(\mathbf{r},t),\end{aligned} \tag{2a}$$

where $\rho = f\cdot\ell_{\rm pi}^2$ is the dimensionless density and the kinetic coefficients are

$$\alpha(\rho) = G - \beta_1\rho(\mathbf{r},t), \tag{2b}$$

$$\kappa(\rho) = -(\beta_2 + \beta_3)\rho(\mathbf{r},t), \tag{2c}$$

$$\beta_1 = a\bar{a}\tilde{c}_2, \tag{2d}$$

$$\beta_2 = a^2\bar{a}^2\tilde{c}_4/4, \tag{2e}$$

$$\beta_3 = (a\bar{a}^3 + \bar{a}a^3)\tilde{c}_4/6, \tag{2f}$$

where $\bar{a} = 1 - a$. Note that all $\beta_i > 0$. The numerical constants $\tilde{c}_k$ are given in Table I. In Eq. 2(a), we rescaled coordinates by the pili length $\ell_{\rm pi}$, i.e., $\mathbf{r} \to \mathbf{r}\ell_{\rm pi}$, leading to a rescaling of time $t \to t\ell_{\rm pi}^2/(\mathcal{W}_0\gamma)$. We introduce the dimensionless parameter,

$$G = \frac{D}{\gamma\mathcal{W}_0}, \tag{2g}$$

with $D = 3\mathcal{K}_0\ell_{\rm pi}^2$ denoting the single cell diffusion constant. G is reminiscent of the inverse Péclet number and can be

TABLE I. The numerical numbers $\tilde{c}_k$ [as defined in Appendix B, Eq. (B6)] corresponding to pili-mediated interactions and adhesion [refer to Eq. (1f) and Eq. (7) for the respective collision kernels].

k	0	1	2	3	4
$\tilde{c}_{k,\rm pi}$	1	0	3	0	45
$\tilde{c}_{k,\rm ad}$	1	0	$\frac{1}{2}$	0	$\frac{3}{4}$

interpreted as a measure for the rate of diffusive particle transport relative to the frequency of interactions. In other words, given a time period between two successive collisions, G quantifies how much distance is traveled (on average) by diffusion with respect to the mean-free path.

An equation similar to Eq. (2a) but phenomenologically constructed appeared in the context of laminar flames and propagation of concentration waves referred to as the Kuramoto-Sivashinsky equation [35,36]. It has also been pointed out as an appropriate framework to study instabilities in growing yeast colonies [6]. However, Eq. (2a) is distinctively different because the kinetic coefficients depend on density [Eqs. (2b) and (2c)]. Moreover, Eq. (2a) exhibits an alleged similarity to the Cahn-Hilliard equation studied in the context of liquid-liquid demixing [37]. Though both equations have terms of similar orders in $\mathcal{O}(\nabla\rho)$, they are fundamentally different with respect to the saturation of droplet or colony growth. The Cahn-Hilliard equation exhibits an instability of the homogeneous state, which saturates because the effective diffusion constant in front of the Laplace operator decreases to zero. Equation (2a) also exhibits an instability but it saturates due to a different mechanism as discussed in the next section.

IV. COLONY FORMATION DUE TO PILI-MEDIATED INTERACTION

A. Onset and saturation of colony formation

Equation (2a) becomes unstable for $\alpha(\rho) < 0$ marking a critical density, $\rho_c = G/\beta_1$. For $\rho_0 > \rho_c$, the homogenous state of density ρ_0 is unstable. The instability enhances small density modulations around the homogenous density ρ_0 with a dispersion relation $w(q) = -\alpha(\rho_0)q^2 - \kappa(\rho_0)q^4$. ρ_c depends on the nondimensional parameter G and the interaction strength a, $\rho_c = G/(a\tilde{a}\tilde{c}_2)$. We find that ρ_c decreases for stronger attractive interactions, $a \to 1/2$, and smaller values of G; see Figs. 2(a), 2(b).

The instability is opposed by fluxes related to the spatial curvature of the density field, which can be qualitatively understood by splitting the flux $\mathbf{j}$ in

$$\partial_t \rho = -\nabla \cdot \mathbf{j} \tag{3a}$$

into three contributions:

$$\mathbf{j} = \mathbf{j}_{\text{inst}} + \mathbf{j}_{\text{cu}} + \mathbf{j}_{\nabla\text{cu}}. \tag{3b}$$

$\mathbf{j}_{\text{inst}} = -\alpha(\rho)\nabla\rho$ denotes the instability flux, which acts for $\alpha < 0$ like negative diffusion thus driving particles to the center of a density spot [see Fig. 2(c) for an illustration]. There the instability current is opposed by the curvature flux, $\mathbf{j}_{\text{cu}} = -\beta_2(\nabla^2\rho)\nabla\rho$, and the gradient-curvature flux, $\mathbf{j}_{\nabla\text{cu}} = (\beta_2 + \beta_3)\rho\nabla(\nabla^2\rho)$. Both are directed outwards of the density spot since curvature is negative and increases.

B. Numerical analysis

Our findings on the instability and its saturation can be scrutinized by numerically [38,39] solving Eq. (2a). A representative snapshot of a state at large time scales is shown in Fig. 1(b) (Videos in the Supplemental Material [29]), which appears to be similar to *N. gonorrhoeae* colonies three hours after sedimentation on a plastic substrate [Fig. 1(a)]. Using parameter values consistent with the experimental system we observe multiple colonies developing quickly for densities above the critical value. We checked numerically that for all parameter values lying within the colony phase of the analytic phase diagram [Figs. 2(a), 2(b)] give rise to the formation of colonies. After the onset of the instability, colonies exponentially grow with a growth speed that is higher the larger the difference of the homogeneous density ρ_0 to the critical density ρ_c; see Figs. 3(a), 3(b). Thus, for $\rho_0 \searrow^+ \rho_c$, we observe a colony growth rate decreasing to zero; a phenomena reminiscent of critical slowing down in phase transitions [40]. Subsequent to the initial growth, there is a regime where colonies grow only very slowly [Fig. 2(d), solid red line] and vanishes when there is only a single colony left in the system [see Figs. 3(c), 3(d)]. The slow growth is due to a weak interaction between the colonies via some evaporation-condensation mechanism qualitatively reminiscent of Ostwald ripening in liquid-liquid phase separation [37]. Interestingly, at the onset of the instability the nonlinear curvature flux $\mathbf{j}_{\text{cu}}$ vanishes

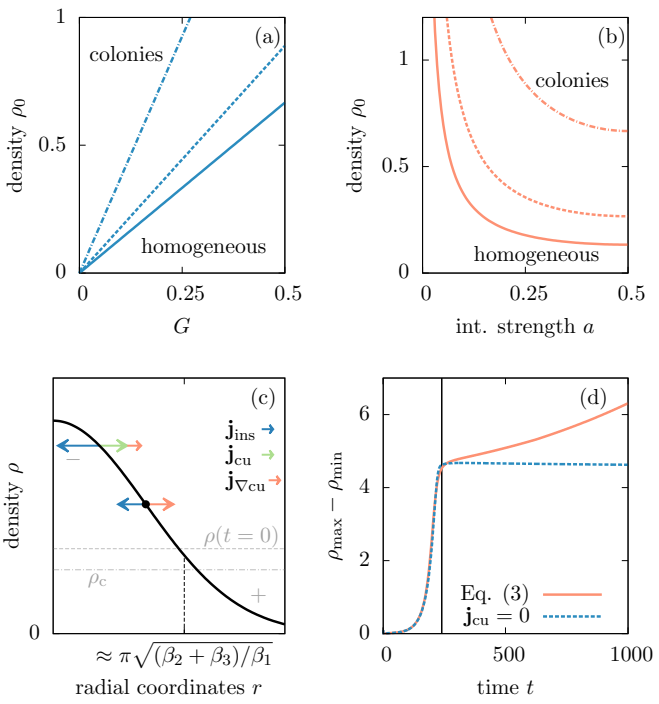

FIG. 2. (Color online) (a), (b) Critical density ρ_c as a function of the nondimensional parameter G and interaction strength a. Each line separates the parameter space, where colonies develop or the system remains homogeneous. In (a), three values of interaction strength a are displayed: (0.5,0.25,0.1) = (solid, dashed, dash-dotted), and (b) depicts three values of G: (0.1,0.2,0.5) = (solid, dashed, dash-dotted). (c) Illustration of how the instability is balanced: For initial densities $\rho(t=0) > \rho_c$, the instability flux $\mathbf{j}_{\text{ins}}$ drives the emergence of a spatially inhomogeneous density profile. Depending on the location along the density profile, the curvature flux $\mathbf{j}_{\text{cu}}$ and/or the gradient curvature flux $\mathbf{j}_{\nabla\text{cu}}$ acts against the instability flux $\mathbf{j}_{\text{ins}}$ and thereby balances the instability. (d) Maximal density minus minimal density, $\rho_{\max} - \rho_{\min}$, as a function of time t, where $\rho_{\max}(t) = \max_{\mathbf{r}}\rho(\mathbf{r},t)$ and $\rho_{\min}(t) = \min_{\mathbf{r}}\rho(\mathbf{r},t)$, for numerical solutions to Eq. (3) with and without curvature flux $\mathbf{j}_{\text{cu}}$.

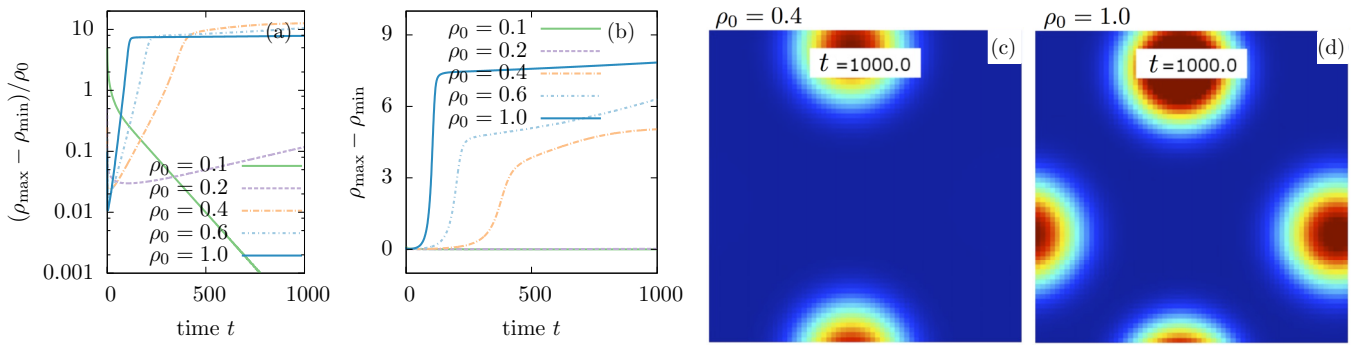

FIG. 3. (Color online) (a), (b) Maximal density minus minimal density, $\rho_{max} - \rho_{min}$, as a function of time t, where $\rho_{max}(t) = \max_{\mathbf{r}} \rho(\mathbf{r},t)$ and $\rho_{min}(t) = \min_{\mathbf{r}} \rho(\mathbf{r},t)$. In (a) we divide through the mean density, $\rho_0 = L^{-2} \int d\mathbf{r} \rho(\mathbf{r},t)$, where L is the system size (here we used $L = 20$). Note that for all numerical runs, ρ is conserved. For the numerical results (a)–(d) we used $a = 0.5$, $G = 0.1$ and consider pili-mediated interactions ($\tilde{c}_2 = 3$), implying a critical density of $\rho_c = G/\beta_1 = 2/15 = 0.13\bar{3}$. (a) Consistently, realizations with $\rho > \rho_c$ exhibit an instability, i.e., $\rho_{max} - \rho_{min}$ grows as a function of time, whereas for $\rho_0 < \rho_c$, weak initial spatial perturbations around ρ_0 decay exponentially. The growth roughly follows an exponential with a speed strongly dependent on the difference of ρ_0 to the critical density: The larger this difference, the faster the initial growth speed. Please note that for densities slightly above the critical threshold (e.g., $\rho_0 = 0.2$), the instability grows too slowly to capture the long time behavior. However, for large enough densities [e.g., $\rho_0 = (0.4, 0.6, 1.0)$], $\rho_{max} - \rho_{min}$ clearly indicates a saturation. (b) The behavior at very large time scales is very hard to capture numerically: Interestingly, if the system has developed to a single colony, $\rho_{max} - \rho_{min}$ becomes flat [see $\rho_0 = 0.4$ and snapshot (c)]. If there are two or more colonies in the system [e.g., $\rho_0 = (1.0)$ and snapshot (d)], $\rho_{max} - \rho_{min}$ still changes as a function of time, though very weakly.

suggesting that it might play an essential role for developed colonies at large time scales. Running the system without curvature flux, $\mathbf{j}_{cu} = 0$ in Eq. (3), we find that the subsequent ripening is absent leading to a stable state consisting of multiple colonies [see Fig. 2(d), dashed line]. This implies that interactions between colonies are driven by the curvature flux, while the gradient curvature flux suffices for the saturation.

C. Estimation of quasistationary colony size

Based on this insight we can analytically estimate the colony size at the time when the system crosses to the very slow ripening regime [vertical line in Fig. 2(d)] by neglecting the curvature flux, $\mathbf{j}_{cu} = \beta_2 (\nabla^2 \rho) \nabla \rho$ in Eq. (3). Note that the curvature flux also vanishes after linearization of Eq. (3) around ρ_0 with $\rho = \rho_0 + \delta\rho$. Assuming quasistatic conditions, $\mathbf{j} = 0$, leads to

$$0 = [\alpha(\rho_0) + \kappa(\rho_0)\nabla^2]\nabla\delta\rho. \tag{4}$$

Within this quasistatic approximation there are two stationary states: The homogenous density field $\rho = \rho_0$ with $\nabla\rho = 0$ and an inhomogeneous state ($\nabla\rho \neq 0$) that supports periodic solutions suggesting the coexistence of several colonies. Since our simulations indicate that droplets are of very similar size when the system crosses from the fast initial growth to the slow ripening phase (see video material), let us approximate the droplet size distribution to be infinitely narrow and extract a single length scale, referred to as quasistationary colony size ξ. Writing $\nabla \to i\mathbf{q}$ and $\xi = \pi |\mathbf{q}|^{-1}$, one finds for $\nabla\rho \neq 0$:

$$\xi^2(\rho_0) \simeq \pi^2 \frac{\kappa(\rho_0)}{\alpha(\rho_0)}. \tag{5}$$

For large densities, $\rho \gg \rho_c$, one gets

$$\xi(\rho_0 \to \infty) \simeq \pi \sqrt{\frac{\beta_2 + \beta_3}{\beta_1}}, \tag{6}$$

which gives approximately 5 pili length for $a = 0.5$; a value that is consistent with *N. gonorrhoeae* [Fig. 1(a)].

D. Biological relevance

In principle, all parameters entering the kinetic description Eq. (1) can be measured or estimated for living colonies forming on a substrate and thereby all kinetic coefficients in Eq. (2a). In particular, for *N. gonorrhoeae*, $\ell_{pi} \approx 1\ \mu$m [9,30] and colony formation is observed for densities of $\rho \approx 0.2$. The attachment rate to the substrate can be obtained from measurements of the single cell diffusion constant, $\mathcal{K}_0 = D/(3\ell_{pi}^2) \approx (6\text{s})^{-1}$ with $D \approx 0.5\ \mu\text{m}^2/\text{s}$ [4] and the cell-cell interaction rate can be roughly estimated from the experimental value of the mean next-neighbor distance and the mean pili number per cell to $\mathcal{W}_0/\ell_{pi}^2 \sim 5\text{s}^{-1}$ (see Appendix D for more information on the estimate). Therefore, a typical value for the dimensionless parameter for *N. gonorrhoeae* is $G \sim 0.1\gamma^{-1}$. Recently, the attachment probability of pili to a substrate has been determined by fitting a model to experimental results [9], finding an approximate value of 0.5. We expect a roughly similar, maybe lower, value for γ since successful binding to another cell can be hindered by other moving cells. So far an appropriate estimate for the interaction strength a is missing because the synchronous visualization of pili and cell movement is not feasible for large enough time scales. Thereby, we consider a as an unknown parameter.

V. COMPETITION OF PILI-MEDIATED AND ADHESIVE INTERACTIONS

A. Competition during colony formation

The proposed kinetic description, Eq. (1), can also be used to include other attractive interactions such as adhesion. Since cell-cell adhesion constitutes a local interaction on the scale of the cell diameter, an appropriate weight function is for example

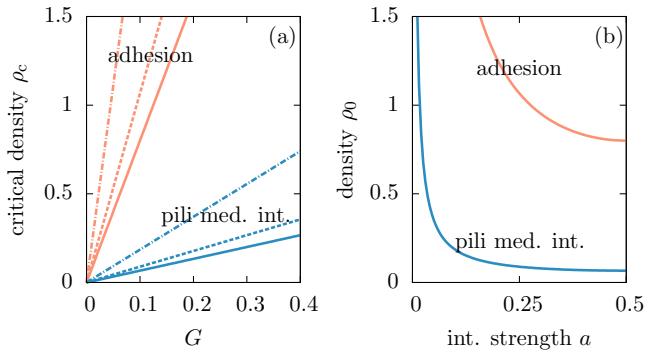

FIG. 4. (Color online) (a), (b) Critical density ρ_c as a function of the non-dimensional parameter G and interaction strength a for pili-mediated interactions (blue, lower right corner) and adhesion (red, upper left corner). In (a), three values of interaction strength a are displayed: (0.5,0.25,0.1) = (solid,dashed,dash-dotted), $\ell_{pi} \approx 2 \cdot \ell_{ad}$ and in (b), $G = 0.1$.

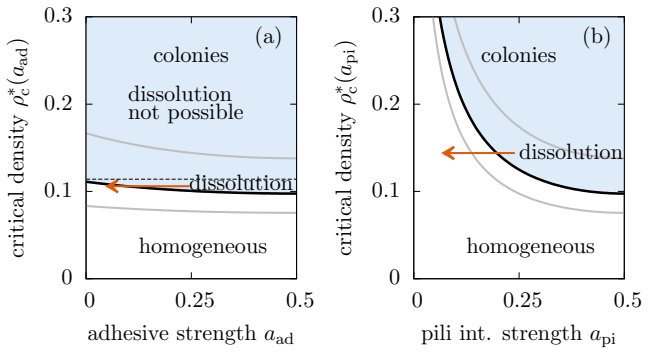

FIG. 5. (Color online) Critical density $\rho_c^*(a_{ad},a_{pi})/G$ as a function of (a) adhesive strength a_{ad} (with $a_{pi} = 0.5$) and (b) pili-mediated interaction strength a_{pi} (with $a_{ad} = 0.5$). In both plots, $G = 0.1$ and each solid line corresponds to $\gamma \in (0.4,0.3,0.2)$ from top to bottom. Black line corresponds to $\gamma = 0.3$. The horizontal black dashed line [plotted only for $\gamma = 0.3$ in (a)] marks the dissolution boundary: Below, dissolution (horizontal red arrow) is possible, above not. Blue shaded areas correspond to the colony phase.

a Gaussian of the form

$$\mathcal{W}_\square \equiv \mathcal{W}_{ad}(|\mathbf{r}_{12}|/\ell_{ad}) = \mathcal{W}_0/\left(\pi \ell_{ad}^2\right) \exp\left(-\mathbf{r}_{12}^2/\ell_{ad}^2\right), \quad (7)$$

where ℓ_{ad} denotes the characteristic length scale, which is in the order of the cell size. Comparing both interactions we find that pili allow for a significantly more pronounced affinity for colony formation compared to adhesive interactions, i.e., colonies already form at smaller initial density of cells [Figs. 4(a), 4(b)]. The reason is that the pili length distribution exhibits a more pronounced tail than the localized Gaussian distribution (characterized by larger $\tilde{c}_2$) and also a larger characteristic length as for *N. gonorrhoeae* ($\ell_{pi} > \ell_{ad}$).

B. Colony dissolution

Many bacteria are known to interact simultaneously by adhesion and pili. It is hypothesized that these bacteria are able to switch off either adhesion or the pili-mediated interaction without affecting their ability to move [16,17,41]. Now we address the question: Can colonies dissolve by switching off either one of these interactions? In other words, given the phase diagram of a specific bacterial system, we discuss some possible means of leaving the colony phase by $a_{pi} \to 0$ or $a_{ad} \to 0$. We now include both interactions by adding a term for pili-mediated interactions $\mathcal{C}_{int,pi}$ and a term corresponding to adhesive interactions $\mathcal{C}_{int,ad}$ on the right-hand side of Eq. (1a), i.e., $\mathcal{C}_{int} = \mathcal{C}_{int,pi} + \mathcal{C}_{int,ad}$. In addition to the already introduced different length scales ℓ_{pi} and ℓ_{ad}, we also distinguish the corresponding interaction strengths, denoted as a_{pi} and a_{ad} (values for adhesion and pili-mediated interactions are denoted as $\tilde{c}_{k,ad}$ and $\tilde{c}_{k,pi}$). We rescale coordinates, density, and time by the adhesive interaction length ℓ_{ad} (or cell size), i.e., $\mathbf{r} \to \mathbf{r} \cdot \ell_{ad}$, $f \to f/\ell_{ad}^2 \equiv \rho$ and $t \to t\ell_{ad}^2/\mathcal{W}_0$, thereby introducing a ratio of these length scales, $\epsilon = \ell_{pi}/\ell_{ad}$. For the case where cells interact with both adhesive and pili-mediated interactions, we find the following effective diffusion constant (for further coefficients see Appendix C):

$$\alpha(\rho) = G - \rho(a_{ad}\bar{a}_{ad}\,\tilde{c}_{2,ad} + a_{pi}\bar{a}_{pi}\,\tilde{c}_{2,pi}\,\gamma\,\epsilon^2). \quad (8)$$

Setting this equation equal to zero marks a critical density

$$\rho_c^*(a_{ad},a_{pi}) = \frac{G}{a_{ad}\bar{a}_{ad}\,\tilde{c}_{2,ad} + a_{pi}\bar{a}_{pi}\,\tilde{c}_{2,pi}\,\gamma\,\epsilon^2} \quad (9)$$

that depends on the strength of both interactions, a_{ad} and a_{pi}.

In order to study the impact of both interactions for dissolution of colonies we choose the parameters $(\epsilon,\ \gamma)$ relevant to *N. gonorrhoeae*. Figure 5(a) shows $\rho_c^*(a_{ad})$ as a function of a_{ad} for $a_{pi} = 0.5$ and $G = 0.1$, while Fig. 5(b) depicts $\rho_c^*(a_{pi})$ as a function of a_{pi} for $a_{ad} = 0.5$ and $G = 0.5$, both for several values of γ. For a given γ, there are two qualitatively distinct regimes for the case where adhesive interactions are switched off [Fig. 5(a)]: For small enough ρ_c^* below the dissolution boundary (horizontal dashed line), colonies can dissolve by switching off the adhesive interaction ($a_{ad} \to 0$) and is indicated by an red arrow. However, above the dissolution boundary, colonies cannot dissolve. Interestingly, choosing the parameters relevant to *N. gonorrhoeae* gives a rather small density regime, where colonies can dissolve, rendering the dissolution scenario through switching off adhesion as a nonrobust mechanism. This is in stark contrast to the scenario of switching off pili-mediated interactions [Fig. 5(b)]: For a given γ, dissolution is possible for all experimental densities in the colony phase by lowering the pili-interaction strength, $a_{pi} \to 0$. These findings suggest that switching off pili-mediated interactions is a more robust mechanism for the dissolution of bacterial colonies than switching off adhesion.

VI. CONCLUSION

To summarize, the formation of living colonies is investigated using a hydrodynamic equation derived from a kinetic description, where most of the parameters can be estimated from experimental data for *N. gonorrhoeae* bacteria. Our results demonstrate that kinetic theory can be successfully used to describe complex far from equilibrium systems such as formation and dissolution of living bacterial colonies. Applications of this theory could pave the way for the physical

quantification of the initial stages of biofilm formation. Though biological reasons for colony formation are specific to each system there are qualitative similarities [1–6]: Colonies form due to encounters with nearby individuals giving rise to structures of a characteristic size determined by the intraspecies interactions and the environment. These similarities suggest that our kinetic description might be applied to other colony-forming systems while the kinetic coefficients in the resulting hydrodynamic equation may differ for each system. Further open questions concern the role of cell division and stochastic fluctuations in living colonies [42].

ACKNOWLEDGMENTS

We thank Igor S. Aranson, Frank Jülicher, and Florian Thüroff for their very insightful comments on this manuscript, and Coleman Broaddus for his careful revisions. We acknowledge funding from the NIH (Grant No. SC2AI116566).

APPENDIX A: COORDINATE CHANGE DUE TO ISOTROPY OF INTERACTION KERNEL

Using the collision rule [Fig. 6],

$$(\mathbf{r}_1,\mathbf{r}_2) \to (\mathcal{R}_1,\mathcal{R}_2) = (\mathbf{r}_1 - a\,\mathbf{r}_{12}, \mathbf{r}_2 + a\,\mathbf{r}_{12}), \tag{A1}$$

the gain term $\mathcal{C}^+$ can be written as:

$$\mathcal{C}^+ = \int d\mathbf{r}_1 \int d\mathbf{r}_2\, \mathcal{W}_\square(\mathbf{r}_1,\mathbf{r}_2)\, f(\mathbf{r}_1,t) f(\mathbf{r}_2,t) \times \frac{1}{2}(\delta[(\mathbf{r}_1 - a\cdot\mathbf{r}_{12}) - \mathbf{r}] + \delta[(\mathbf{r}_2 + a\cdot\mathbf{r}_{12}) - \mathbf{r}]). \tag{A2}$$

The equation above can be rewritten in terms of relative coordinates $\mathbf{r}_{12} = \mathbf{r}_1 - \mathbf{r}_2$ and center-of-mass coordinates $\mathbf{R}_{12} = (\mathbf{r}_1 + \mathbf{r}_2)/2$, i.e., $\mathbf{r}_1 = \mathbf{R}_{12} + \mathbf{r}_{12}/2$ and $\mathbf{r}_2 = \mathbf{R}_{12} - \mathbf{r}_{12}/2$ (Fig. 6):

$$\mathcal{C}^+ = \frac{1}{2}\int d\mathbf{r}_{12} \int d\mathbf{R}_{12}\, \mathcal{W}_\square(|\mathbf{r}_{12}|) \times f(\mathbf{R}_{12} + \mathbf{r}_{12}/2,t) f(\mathbf{R}_{12} - \mathbf{r}_{12}/2,t) \times \left\{\delta\left[\mathbf{R}_{12} + \mathbf{r}_{12}\left(\frac{1}{2} - a\right) - \mathbf{r}\right] + \delta\left[\mathbf{R}_{12} + \mathbf{r}_{12}\left(-\frac{1}{2} + a\right) - \mathbf{r}\right]\right\}. \tag{A3}$$

Due to the isotropy of the collision kernel the integration over the center-of-mass coordinates can be performed, finding

$$\mathcal{C}^+ = \frac{1}{2}\int d\mathbf{r}_{12}\, \mathcal{W}_\square(|\mathbf{r}_{12}|)[f(\mathbf{r} + a\mathbf{r}_{12},t) f(\mathbf{r} - \bar{a}\mathbf{r}_{12},t) + f(\mathbf{r} - a\mathbf{r}_{12},t) f(\mathbf{r} + \bar{a}\mathbf{r}_{12},t)], \tag{A4}$$

where $\bar{a} = 1 - a$. The equation above can be further simplified for example for the case $a = \frac{1}{2}$:

$$\mathcal{C}^+ = \int d\mathbf{r}_{12}\, \mathcal{W}_\square(|\mathbf{r}_{12}|) f(\mathbf{r} + \mathbf{r}_{12}/2,t) f(\mathbf{r} - \mathbf{r}_{12}/2,t). \tag{A5}$$

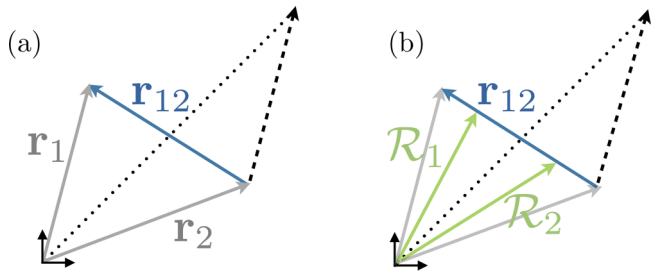

FIG. 6. (Color online) Illustration of collision setup and the collision rule mimicking attractive interactions. (a) The two collision partners have the spatial coordinates $\mathbf{r}_1$ and $\mathbf{r}_2$, defining a relative distance $\mathbf{r}_{12} = \mathbf{r}_1 - \mathbf{r}_2$ and a center-of-mass coordinate $\mathbf{R}_{12} = (\mathbf{r}_1 + \mathbf{r}_2)/2$. (b) The collision given in Eq. (2) (main text), which maps the precollision coordinates $(\mathbf{r}_1,\mathbf{r}_2)$ to the postcollision coordinates $(\mathcal{R}_1(\mathbf{r}_1,\mathbf{r}_2),\mathcal{R}_2(\mathbf{r}_1,\mathbf{r}_2))$ (indicated by green arrows). For the illustration, $a = 0.25$.

Similar manipulations can be performed for the loss term:

$$\begin{aligned}\mathcal{C}^- &= \int d\mathbf{r}_1 \int d\mathbf{r}_2\, \mathcal{W}_\square(|\mathbf{r}_{12}|)\, f(\mathbf{r}_1,t) f(\mathbf{r}_2,t)\, \delta(\mathbf{r}_2 - \mathbf{r}) \\ &= \int d\mathbf{r}_{12} \int d\mathbf{R}_{12}\, \mathcal{W}_\square(|\mathbf{r}_{12}|)\, \delta[\mathbf{R}_{12} - (\mathbf{r}_{12}/2 + \mathbf{r})] \\ &\quad \times f(\mathbf{R}_{12} + \mathbf{r}_{12}/2,t) f(\mathbf{R}_{12} - \mathbf{r}_{12}/2,t) \\ &= f(\mathbf{r},t) \int d\mathbf{r}_{12}\, \mathcal{W}_\square(|\mathbf{r}_{12}|)\, f(\mathbf{r} + \mathbf{r}_{12}) \\ &\equiv f(\mathbf{r},t) \int d\mathbf{r}_{12}\, \mathcal{W}_\square(|\mathbf{r}_{12}|) f(\mathbf{r} - \mathbf{r}_{12}).\end{aligned} \tag{A6}$$

Please note that nonlocal integrands above resemble a phenomenological description for the assembly of active bundles [32–34].

APPENDIX B: DETAILS OF COARSE GRAINING AND TRUNCATION

Truncating of the nonlocal distribution function $f(\mathbf{r} \pm a\mathbf{r}_{12})$ [cf. Eqs. (A4) and (A6)] at the fourth order leads to

$$f(\mathbf{r} \pm a\mathbf{r}_{12}) = f(\mathbf{r}) \pm a(\mathbf{r}_{12}\cdot\nabla) f(\mathbf{r}) + \frac{a^2}{2}(\mathbf{r}_{12}\cdot\nabla)^2 f(\mathbf{r}) \pm \frac{a^3}{6}(\mathbf{r}_{12}\cdot\nabla)^3 f(\mathbf{r}) + \frac{a^4}{24}(\mathbf{r}_{12}\cdot\nabla)^4 f(\mathbf{r}) + \mathcal{O}[(\mathbf{r}_{12}\cdot\nabla)^5], \tag{B1}$$

where we omitted the time dependence for reasons of brevity. Using the truncation above and neglecting all terms $\mathcal{O}[(\mathbf{r}_{12}\cdot\nabla)^5]$ amounts to an explicit coarse graining of the system's dynamics to length scales beyond the characteristic length scale of the interaction. Therefore, we will refer to the resulting equation obtained at the end of this section as the hydrodynamic equation.

1. Single cell motility term

The term modeling the single cell motility across the substrate, $\mathcal{C}_{\text{mot}}$, can be coarse grained as follows: Defining the pili-mediated displacement as $\mathbf{b} = (b_x,b_y) = \mathbf{r}' - \mathbf{r}$, and

the transition rate $\mathcal{K}_{\mathbf{r}\to\mathbf{r}'} \equiv \mathcal{K}(\mathbf{b};\mathbf{r})$,

$$\begin{aligned}\mathcal{C}_{\rm mot}(\mathbf{r},t) &= \int d\mathbf{r}'[\mathcal{K}_{\mathbf{r}'\to\mathbf{r}} f(\mathbf{r}',t) - \mathcal{K}_{\mathbf{r}\to\mathbf{r}'} f(\mathbf{r},t)] \\ &= \int d\mathbf{b}[\mathcal{K}(-\mathbf{b};\mathbf{r}+\mathbf{b}) f(\mathbf{r}',t) - \mathcal{K}(\mathbf{b};\mathbf{r}) f(\mathbf{r},t)] \\ &= \int d\mathbf{b}[\mathcal{K}(\mathbf{b};\mathbf{r}-\mathbf{b}) f(\mathbf{r}-\mathbf{b},t) - \mathcal{K}(\mathbf{b};\mathbf{r}) f(\mathbf{r},t)].\end{aligned} \tag{B2}$$

Expanding the nonlocal integrand with respect to the spatial coordinates and keeping only the highest nonvanishing order leads to:

$$\begin{aligned}\mathcal{C}_{\rm mot}(\mathbf{r},t) &= \int d\mathbf{b}\frac{1}{2}(\mathbf{b}\cdot\nabla)^2[\mathcal{K}(\mathbf{b};\mathbf{r}) f(\mathbf{r},t)] \\ &= \int d\mathbf{b}\frac{1}{2}\mathcal{K}(\mathbf{b})(b_x\partial_x + b_y\partial_y)^2 f(\mathbf{r},t) \\ &= \int d\mathbf{b}\frac{1}{2}\mathcal{K}(\mathbf{b})\left(b_x^2\partial_x^2 + b_y^2\partial_y^2\right) f(\mathbf{r},t) \\ &= \left[\int d\mathbf{b}\mathcal{K}(|\mathbf{b}|)b_x^2\right]\left(\partial_x^2 + \partial_y^2\right) f(\mathbf{r},t) \\ &= D\nabla^2 f(\mathbf{r},t),\end{aligned} \tag{B3}$$

where we assumed that the transition rate does not depend on the spatial coordinates, $\mathcal{K}(\mathbf{b};\mathbf{r}) = \mathcal{K}(\mathbf{b})$, and that it is an even [43] and isotropic function, $\mathcal{K}(\mathbf{b}) = \mathcal{K}(|\mathbf{b}|)$. Moreover, using $\mathcal{K}(|\mathbf{b}|) = \mathcal{K}_0 \frac{1}{2\pi\ell_{\rm pi}^2}\exp(-|\mathbf{b}|/\ell_{\rm pi})$ one obtains the diffusion constant for pili-mediated motility:

$$D = \mathcal{K}_0\ell_{\rm pi}^2\tilde{c}_{2,\rm pi}, \tag{B4}$$

where $\tilde{c}_{2,\rm pi}$ given in Table I and $\mathcal{K}_0$ denotes the attachment rate of pili to the substrate. Restricting to the second order is validated by the *Pawula* theorem [44].

2. Interaction term

The interaction term $\mathcal{C}_{\rm int}$ can be split in a gain term, $\mathcal{C}^+$, and a loss term, $\mathcal{C}^-$.

Loss. Neglecting all terms above the fourth order, we find for the loss term:

$$\mathcal{C}^- = f(\mathbf{r})\left[c_0 f(\mathbf{r}) + \frac{c_2}{2}\nabla^2 f(\mathbf{r}) + \frac{c_4}{24}\nabla^4 f(\mathbf{r})\right], \tag{B5}$$

where the coefficients are given as

$$\begin{aligned}c_k &= \iint dr_{12,x}dr_{12,y}\, r_{12,x}^k\, \mathcal{W}_{\rm ad/pi}(r_{12}) \\ &= \mathcal{W}_0\begin{cases}\ell_{\rm ad/pi}^k\cdot\tilde{c}_k & \text{if } k \text{ even},\\ 0 & \text{if } k \text{ odd},\end{cases}\end{aligned} \tag{B6}$$

with $r_{12} = |\mathbf{r}_{12}| = \sqrt{r_{12,x}^2 + r_{12,y}^2}$ and $\tilde{c}_k$ are dimensionless numbers given in Table I for the adhesive (ad) and pili-mediated (pi) interaction. Note that odd powers, thereby also mixed gradients such as $\partial_x\partial_y f$, vanish since the integral is then an asymmetric function with respect to the integration over e.g. $dr_{12,x}$ or $dr_{12,x}$, respectively [45].

Gain. Following similar lines for the source term $\mathcal{C}^+$, and neglecting all contributions above the fourth order in the spatial derivatives, we find only six nonzero contributions:

$$\begin{aligned}\mathcal{C}^+ = {} & c_0 f^2(\mathbf{r}) + \tfrac{1}{2}[a^2+\bar{a}^2]c_2 f(\mathbf{r})\nabla^2 f(\mathbf{r}) - a\bar{a}c_2|\nabla f(\mathbf{r})|^2 \\ & + \tfrac{1}{24}[a^4+\bar{a}^4]c_4 f(\mathbf{r})\nabla^4 f(\mathbf{r}) + \tfrac{1}{4}a^2\bar{a}^2c_4[\nabla^2 f(\mathbf{r})]^2 \\ & - \tfrac{1}{6}[a\bar{a}^3+\bar{a}a^3]c_4[\nabla f(\mathbf{r})]\cdot\nabla^3 f(\mathbf{r}).\end{aligned} \tag{B7}$$

Gain and loss. Combining gain and loss term, $\mathcal{C}_{\rm int} = \mathcal{C}^+ - \mathcal{C}^-$, and plugging it in Eq. (1) (main text), leads to the final hydrodynamic equation:

$$\begin{aligned}\partial_t f(\mathbf{r},t) = {} & D\nabla^2 f(\mathbf{r},t)] + \tfrac{1}{2}[a^2+\bar{a}^2-1]c_2 f(\mathbf{r},t)\nabla^2 f(\mathbf{r},t) \\ & + \tfrac{1}{24}[a^4+\bar{a}^4-1]c_4 f(\mathbf{r},t)\nabla^4 f(\mathbf{r},t) \\ & - a\bar{a}c_2|\nabla f(\mathbf{r},t)|^2 + \tfrac{1}{4}a^2\bar{a}^2c_4[\nabla^2 f(\mathbf{r},t)]^2 \\ & - \tfrac{1}{6}[a\bar{a}^3+\bar{a}a^3]c_4[\nabla f(\mathbf{r},t)]\cdot\nabla^3 f(\mathbf{r},t).\end{aligned} \tag{B8}$$

Note that in Eq. (B8) the zeroth-order term cancels because of particle conservation.

As the last step, we use the scaling of the kinetic coefficients, $c_k = \mathcal{W}_0\ell^k\tilde{c}_k$ [see Eq. (B6)], with $\ell \in \{\ell_{\rm ad},\ell_{\rm pi}\}$ and the numerical values $\tilde{c}_k$ given in Table I, and write Eq. (B8) in a dimensionless form. To this end, we rescale the coordinates and the density by means of the interaction length ℓ, i.e., $\mathbf{r}\to\mathbf{r}\cdot\ell$ and $f\to f/\ell^2 \equiv \rho$. This implies a rescaling of the time scale given by $t\to t\ell^2/(\mathcal{W}_0\gamma)$; note that $\gamma = 1$ for adhesive interactions. Using the aforementioned rescalings leads to Eq. (2a).

APPENDIX C: KINETIC COEFFICIENTS FOR ADHESION AND PILI-MEDIATED INTERACTIONS

For adhesive and pili-mediated interactions, only the effective diffusion constant $\alpha(\rho)$ has been given in the main text. Reading the coefficients Eqs. (2d)–(2f) as function of the interaction strength a, i.e., $\beta_i = \beta_i(a)$, the remaining coefficient is listed below:

$$\kappa(\rho) = -\{[\beta_2(a_{\rm ad}) + \beta_3(a_{\rm ad})] + [\beta_2(a_{\rm pi}) + \beta_3(a_{\rm pi})]\,\gamma\,\epsilon^4\}. \tag{C1}$$

The corresponding length scales, interaction strength and numerical coefficients for adhesion and pili-mediated interactions are denoted as: $\ell_{\rm pi}, a_{\rm ad}, \tilde{c}_{k,\rm ad}$ and $\ell_{\rm ad}, a_{\rm ad}, \tilde{c}_{k,\rm ad}$, respectively, and $\epsilon = \ell_{\rm pi}/\ell_{\rm ad}$. The rescalings used are described in Sec. V B.

APPENDIX D: ESTIMATES OF PARAMETERS OF THE *N. GONORRHOEAE*

1. Estimate of the density ρ_0

We considered 20 experimental realizations of *N. gonorrhoeae* bacteria forming colony on a substrate. After sedimentation to the plastic surface we calculated from the corresponding binary images the overall area fraction covered by bacteria cells, finding $\phi \approx 0.1$. The corresponding dimensionless density is then: $\rho_0 = \phi\ell_{\rm pi}^2/(\pi R_{\rm cell}) \approx 0.125$ with $\ell_{\rm pi} = 1\ \mu$m and $R_{\rm cell} = 0.5\ \mu$m. Since typically some small three-dimensional colonies have already formed during sedimentation process we expect that the determined value

represents a slight underestimation, thereby we use $\rho_0 = 0.2$ in the manuscript.

2. Estimate of $\mathcal{W}_0/\ell_{\rm pi}^2$

$\mathcal{W}_0/\ell_{\rm pi}^2$ is a measure for the rate of cell-cell encounters occurring in an area of $\ell_{\rm pi}^2$. A direct measurement of this quantity requires the sampling of the cell trajectories on the time-scale of the cell-cell encounters, which is intricate because bacteria cells are harmed in case of too frequent light exposure. Therefore, we have to content ourselves with a rough estimate. If we assume that each pilus per cell acts independently, we can first estimate the rate of a cell-cell interaction for a single pilus. For intermediate and large cell densities with respect to the intersection scales, it is expected that this rate roughly scales with the number of pili per cell.

The time τ between two interactions using a single pilus should be roughly given by the time to diffuse the distance to the next-neighboring cell $\ell_{\rm NN}$, $\tau \sim \ell_{\rm NN}^2/(4D)$, where $D = 0.5\ \mu\text{m}^2/\text{s}$. However, this distance is reduced by the cell-diameter $2R_{\rm cell} = 1\ \mu\text{m}$ and two times the typical pili length $2\ell_{\rm pi} = 2\ \mu\text{m}$ (the factor 2 is based on very recent experimental observation that pili-mediated cell-cell interactions occurs via pili-pili bundling) leading to: $\tau \sim (\ell_{\rm NN} - 2R_{\rm cell} - 2\ell_{\rm pi})^2/(4D) \approx 2\ \text{s}$, where we determined $\ell_{\rm NN} \approx 5\ \mu\text{m}$ from the binary images directly after sedimentation.

TEM-images indicate that the mean pili number is in order of $N \sim 10$ [30]. For intermediate and large cell densities, the overall interaction rate for for *N. gonorrhoeae* at surface coverage of $\phi \approx 0.1$ is approximately $\mathcal{W}_0/\ell_{\rm pi}^2 \sim N(2\text{s})^{-1} \approx 5\text{s}^{-1}$. Thereby, $G \approx 0.1$.

[1] E. Ben-Jacob, I. Cohen, and D. L. Gutnick, Ann. Rev. Microbiol. **52**, 779 (1998).
[2] O. Lejeune, M. Tlidi, and P. Couteron, Phys. Rev. E **66**, 010901 (2002).
[3] D. L. Higashi *et al.*, Infect Immun. **75**, 4743 (2007).
[4] J. Taktikos, Y. T. Lin, H. Stark, N. Biais, and V. Zaburdaev [PLoS ONE (to be published)].
[5] L. Hall-Stoodley, J. W. Costerton, and P. Stoodley, Nat. Rev. Microbiol. **2**, 95 (2014).
[6] T. Sams, K. Sneppen, M. H. Jensen, C. Ellegaard, B. E. Christensen, and U. Thrane, Phys. Rev. Lett. **79**, 313 (1997).
[7] A. J. Merz, M. So, and M. P. Sheetz, Nature (London) **407**, 98 (2000).
[8] R. Marathe *et al.*, Nat. Commun. **5**, 3759 (2014).
[9] V. Zaburdaev *et al.*, Biophys. J. **107**, 1523 (2014).
[10] B. Maier *et al.*, Proc. Nat. Acad. Sci. USA **99**, 16012 (2002).
[11] B. Maier, Soft Matter **9**, 5667 (2013).
[12] L. Craig, M. E. Pique, and J. A. Tainer, Nat. Rev. Microbiol. **2**, 363 (2004).
[13] N. Biais *et al.*, PLoS Biol. **6**, e87 (2008).
[14] B. Westling-Häggström, T. Elmros, S. Normark, and B. Winblad, J. Bacteriol. **29**, 333 (1977).
[15] I. Kolodkin-Gal *et al.*, Science **328**, 627 (2010).
[16] J. Chamot-Rooke *et al.*, Science **331**, 778 (2011).
[17] L. Dewenter, T. E. Volkman, and B. Maier, Integr. Biol. (2015), doi: 10.1039/C5IB00018A
[18] I. S. Aranson and L. S. Tsimring, Phys. Rev. E **71**, 050901 (2005).
[19] E. Bertin, M. Droz, and G. Grégoire, Phys. Rev. E **74**, 022101 (2006).
[20] E. Bertin, M. Droz, and G. Grégoire, J. Phys. A **42**, 445001 (2009).
[21] D. Saintillan and M. J. Shelley, Phys. Rev. Lett. **99**, 058102 (2007).
[22] I. S. Aranson, A. Sokolov, J. O. Kessler, and R. E. Goldstein, Phys. Rev. E **75**, 040901 (2007).
[23] D. Saintillan and M. J. Shelley, Phys. Rev. Lett. **100**, 178103 (2008).
[24] T. Ihle, Phys. Rev. E **83**, 030901 (2011).
[25] F. Thüroff, C. A. Weber, and E. Frey, Phys. Rev. Lett. **111**, 190601 (2013).
[26] C. A. Weber, F. Thüroff, and E. Frey, New J. Phys. **15**, 045014 (2013).
[27] T. Hanke, C. A. Weber, and E. Frey, Phys. Rev. E **88**, 052309 (2013).
[28] F. Thüroff, C. A. Weber, and E. Frey, Phys. Rev. X **4**, 041030 (2014).
[29] See Supplemental Material at http://link.aps.org/supplemental/10.1103/PhysRevE.92.032704 for videos and more information.
[30] Since we focus on the onset of the instability, three-dimensional growth should be of secondary importance.
[31] C. Holz, D. Opitz, L. Greune, R. Kurre, M. Koomey, M. A. Schmidt, and B. Maier, Phys. Rev. Lett. **104**, 178104 (2010).
[32] K. Kruse and F. Jülicher, Phys. Rev. Lett. **85**, 1778 (2000).
[33] K. Kruse and F. Jülicher, Phys. Rev. E **67**, 051913 (2003).
[34] K. Kruse, A. Zumdieck, and F. Jülicher, Europhys. Lett. **64**, 716 (2003).
[35] Y. Kuramoto and T. Tsuzuki, Prog. Theor. Phys. **55**, 356 (1976).
[36] G. Sivashinsky, Acta Astronautica **4**, 1177 (1977).
[37] A. Bray, Adv. Phys. **43**, 357 (1994).
[38] Equation (2a) was solved numerically using an eighth- (embedded ninth-) order adaptive Runge-Kutta method. Specifically, we employed an established package called XMDS2 (see http://www.xmds.org) developed by Graham R. Dennis, Joseph J. Hope, and Mattias T. Johnsson [39].
[39] G. R. Dennis, J. J. Hope, and M. T. Johnsson, Comput. Phys. Commun. **184**, 201 (2013).
[40] A. Onuki, *Phase Transition Dynamics* (Cambridge University Press, Cambridge, 2002).
[41] M. Gjermansen *et al.*, Environ. Microbiol. **7**, 894 (2005).
[42] L. S. Tsimring, Rep. Prog. Phys. **77**, 026601 (2014).
[43] Thereby, odd integrands, e.g., $b_x b_y$, vanish by integration.
[44] N. van Kampen, *Stochastic Processes in Physics and Chemistry* (Elsevier, Amsterdam, 2007).
[45] Assuming that f vanishes at infinity, integration by parts leads to: $(\partial_x\partial_x f)(\partial_y\partial_y f) = (\partial_x\partial_y f)(\partial_x\partial_y f)$.